Storm Reflectivity and Mesocyclone Evolution Associated with the 15 April 1994 Squall Line over Kentucky and Southern Indiana

THEODORE W. FUNK, KEVIN E. DARMOFAL,* JOSEPH D. KIRKPATRICK, AND VAN L. DEWALD

NOAA/National Weather Service Forecast Office Louisville, Louisville, Kentucky

RON W. PRZYBYLINSKI AND GARY K. SCHMOCKER

NOAA/NWS Forecast Office St. Louis, St. Charles, Missouri

YEONG-JER LIN

Department of Earth and Atmospheric Sciences, Saint Louis University, St. Louis, Missouri

(Manuscript received 13 November 1998, in final form 14 May 1999)

ABSTRACT

A long-lived highly organized squall line moved rapidly across the middle Mississippi and Ohio Valleys on 15 April 1994 within a moderately unstable, strongly sheared environment. Over Kentucky and southern Indiana, the line contained several bowing segments (bow echoes) that resulted in widespread wind damage, numerous shear vortices/rotational circulations, and several tornadoes that produced F0–F2 damage. In this study, the Louisville–Fort Knox WSR-88D is used to present a thorough discussion of a particularly long-tracked bowing line segment over central Kentucky that exhibited a very complex and detailed evolution, more so than any other segment throughout the life span of the squall line. Specifically, this segment produced abundant straight-line wind damage; cyclic, multiple core cyclonic circulations, some of which met mesocyclone criteria; several tornadoes; and embedded high precipitation supercell-like structure that evolved into a rotating comma head–comma tail pattern. The bowing segment also is examined for the presence of bookend vortices aloft and midaltitude radial convergence. In addition, the structure of other bowing segments and their attendant circulations within the squall line are discussed and compared with existing documentation. Radar sampling issues and ramifications of the squall line's complicated structure on the warning process of future similar severe weather events are touched upon as well.

1. Introduction

The structure and evolution of convective squall lines have long intrigued meteorologists, particularly the bulging, convex-shaped radar echo patterns that often develop within these lines. Nolen (1959) provided an early reference of these patterns, coining the phrase *line-echo wave pattern* (LEWP), while Hamilton (1970) linked the bulging echoes with damaging straight-line winds. Fujita (1978) then described the morphology of this storm type, terming the system a *bow echo* in which downburst winds caused the echo bulging. Johns and Hirt (1987) studied the derecho, a widespread convectively induced windstorm, which was associated with rapidly moving squall lines and bow echoes. Przybylinski (1995), Przybylinski and Schmocker (1993), Burgess and Smull (1990), and Forbes and Wakimoto (1983) have shown that the strongest downburst winds and most intense damage occur along the apex of bowing line segments. These studies also have revealed that shear vortices/rotational cyclonic circulations can occur along or near the leading bow apex, which can produce tornadoes of F0–F3 intensity.

The development, evolution, and longevity of mature squall lines and embedded bow echoes are dependent on the characteristics of the mesoscale rear inflow jet (e.g., Weisman 1993). However, much documentation on both observed (e.g., Smull and Houze 1987; Rutledge et al. 1988) and simulated convective systems (e.g., Rotunno et al. 1988; Fovell and Ogura 1988; Lafore and Moncrieff 1989; Weisman 1992, 1993) has suggested that the exact interactions of the rear-inflow jet (RIJ) with the environment in dictating squall line evolution can be quite complex. In general, the RIJ is present during the mature stage of a convective system, when

* Current affiliation: NWSO Wichita, Wichita, Kansas.

Corresponding author address: Theodore W. Funk, NWSFO Louisville, 6201 Theiler Lane, Louisville, KY 40229.
E-mail: Theodore.Funk@noaa.gov

a deep convectively induced low-level cold pool overwhelms the environmental wind shear, causing convective updrafts to tilt upshear over the cold dome (Rotunno et al. 1988). As this occurs, horizontal buoyancy gradients between a buoyant rearward-tilted plume aloft and the low-level cold pool generate horizontal vorticity and a circulation that acts to accelerate the RIJ (Lafore and Moncrieff 1989; Weisman 1992). In addition, Weisman (1992) has suggested that the strength and character of the RIJ are dependent on the amount of ambient convective available potential energy (CAPE) and vertical wind shear. The RIJ tends to remain elevated up to the updraft–downdraft interface near the leading convective line, given high amounts of ambient CAPE (at least 2000 J kg^{-1}) and low- to middle-level vertical wind shear (20 m s^{-1} or more). In these situations, strong low-level convergence generates rapid multicellular convective growth, resulting in an organized, relatively long-lived system with embedded bowing line segments. These segments typically cause damaging surface winds and the possible development of rotational cyclonic vortices and tornadoes. In contrast, weakly sheared environments typically are characterized by a descending RIJ and a less organized, shorter-lived system.

These and other documented findings have provided a strong, fundamental understanding of the structure and evolution of bowing line segments associated with squall lines. In recent years, several studies, such as Heinlein et al. (1998), Funk et al. (1998), and DeWald et al. (1998), have used high-resolution Weather Surveillance Radar 1988-Doppler (WSR-88D) data to document squall line and bow echo structure. In addition, Przybylinski et al. (1996) and Funk et al. (1996a) used WSR-88D data to perform a preliminary investigation of the 15 April 1994 squall line across the middle Mississippi and Ohio Valleys. In this event, the mesoscale convective system (MCS) developed late on 14 April over Missouri; exhibited an intense, organized structure as it moved across the Ohio Valley on 15 April; then gradually weakened over the Appalachian Mountains. The derecho-producing MCS contained numerous bowing line segments, widespread wind damage, and several tornadoes throughout much of its life span.

In this paper, 5–6-min interval Louisville–Fort Knox (KLVX) WSR-88D reflectivity and velocity data are used to evaluate the detailed structure and evolution of the 15 April squall line over Kentucky and southern Indiana. Specifically, a thorough discussion is presented of a long-tracked bowing line segment over central Kentucky that exhibited a very complicated and detailed evolution, more so than any other bowing segment during the life cycle of the squall line. This segment produced extensive straight-line wind damage; cyclic, multiple core cyclonic circulations, some of which met mesocyclone criteria; several tornadoes; and embedded high precipitation (HP) supercell-like structure that evolved into a rotating comma head–comma tail pattern. The presence of bookend vortices aloft and midaltitude radial convergence (MARC) within this line segment also is examined. In addition, an evaluation of other shorter-lived bowing segments and their attendant circulations is presented and compared to existing documentation. Finally, the effect of radar sampling issues and ramifications of this case to the overall warning process are discussed briefly as well. It is important to note that only the four lowest KLVX WSR-88D elevation angles (3.4° and below) were available for this study, which prevented high-altitude storm evaluation near the radar. However, this limitation does not detract from the integrity of the results presented in this paper.

2. Preconvective environment

The 1200 UTC 15 April synoptic environment was quite similar to the ''dynamic'' pattern described by Johns (1993), and to ambient conditions at 0000 UTC 15 April (Przybylinski et al. 1996). The squall line moved across the Ohio Valley coincident with low-level thermal and moisture ridge axes, and ahead of a surface cold front and progressive 500-mb trough (Fig. 1). Surface dewpoints immediately ahead of the squall line ranged from 15° to 20°C. A 25 m s^{-1} 850-mb wind maximum caused strong low-level moisture transport and convergence over the lower Ohio Valley at 1200 UTC, with enhanced upper-level divergence located between dual jet streaks (40–45 m s^{-1}) at 300 mb (Fig. 1). The resulting strong environmental forcing was favorable for maintaining the intensity of the convective line.

In the 15 April case, Weisman's (1992) rough CAPE and wind shear criteria for long-lived bowing MCSs were met as a moderate instability–strong shear environment existed across the Ohio Valley. The Paducah, Kentucky, sounding data at 1200 UTC (located just ahead of the squall line at that time) indicated a lifted index of -6 to -8 and a CAPE value of approximately 2400 J kg^{-1} (Fig. 2). At the same time, the vertical wind profile and hodograph from Paducah (Fig. 2) revealed nearly 20 m s^{-1} shear in the 0–2-km layer with relatively weak shear aloft. By 1410 UTC, however, the KLVX WSR-88D vertical wind profile data (Fig. 1) showed 0–2-km shear values of nearly 25 m s^{-1} with quasi-constant winds aloft. Both the sounding and radar-based wind profiles indicated strong speed and only modest directional shear in the lowest 2 km of the atmosphere, a profile associated with bow echo occurrence (Johns 1993). The Paducah sounding also revealed a 0–2-km storm-relative helicity of nearly 300 m^2 s^{-2}, a value associated with possible deep mesocyclone and tornado development (Davies-Jones et al. 1990), and a bulk Richardson number of about 40, a value associated with potential embedded supercell structure (Weisman and Klemp 1982, 1984).

Due to the different wind sensing methodology between radiosonde and radar-derived wind fields, it is

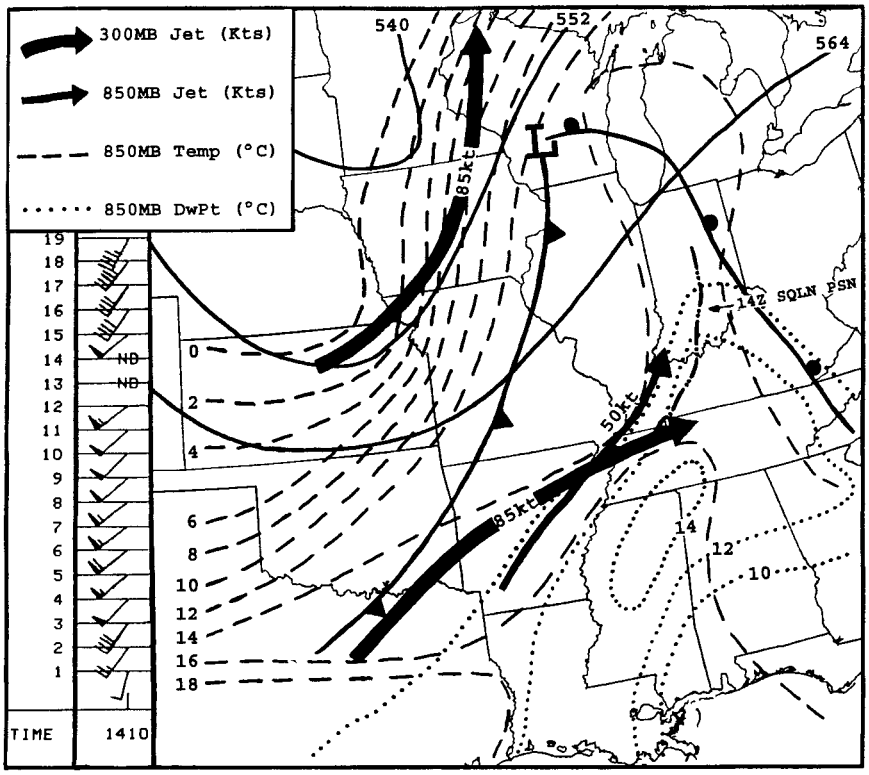

FIG. 1. Composite synoptic chart for 1200 UTC 15 April 1994. Key at upper left identifies 850- and 300-mb parameters. Also shown are surface fronts, 500-mb heights (in dm; thin solid lines), the 1400 UTC squall line position (dashed–dotted line), and the vertical wind profile (in kt and thousands of ft) from the KLVX WSR-88D at 1410 UTC.

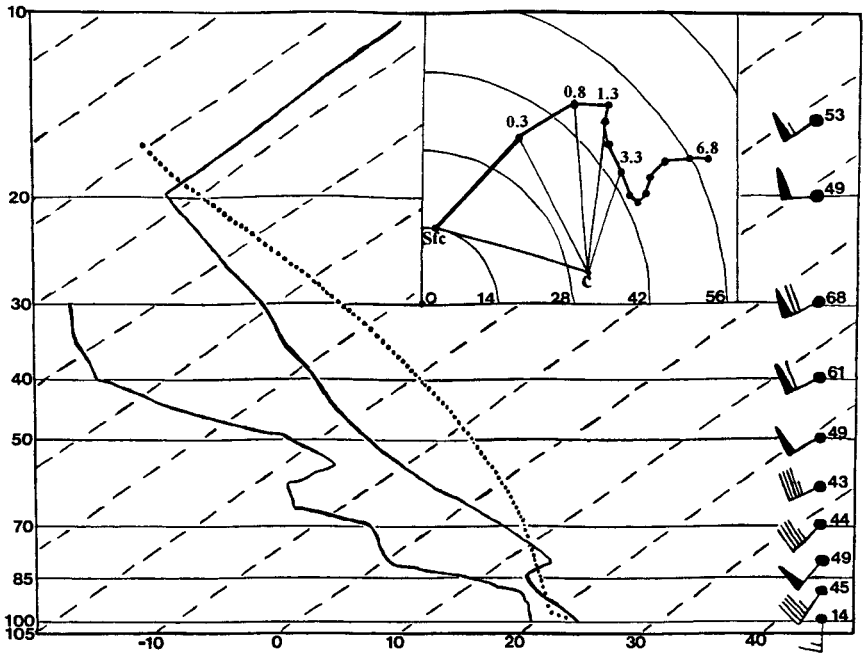

FIG. 2. The Paducah (PAH), KY, skew *T* sounding and hodograph (inset) at 1200 UTC 15 Apr. Winds in kt are shown at right. In the hodograph, numbers along the *x*-axis are wind speeds in kt, numbers along the hodograph curve represent km above the surface, and C is the default storm motion. Key thermodynamic parameters are given in the text.

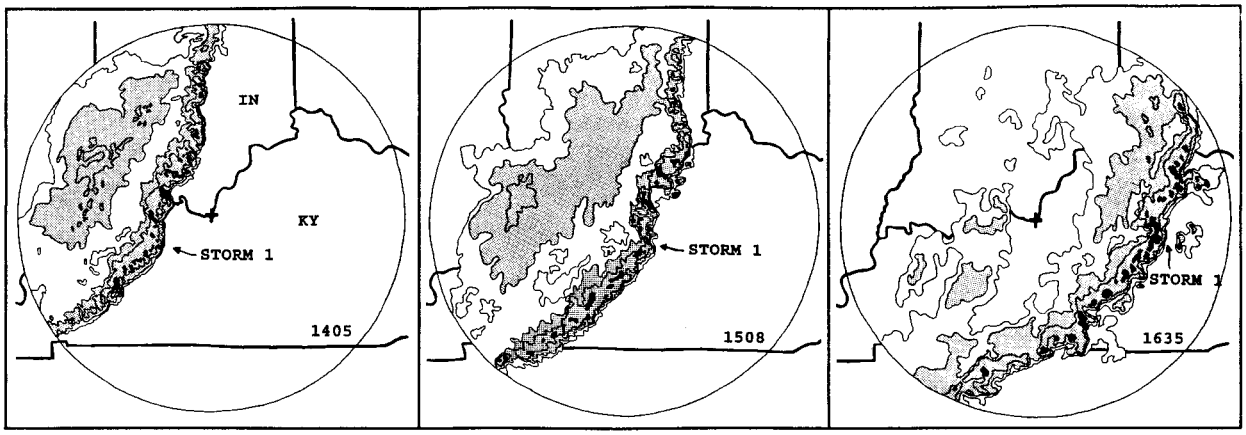

FIG. 3. Base reflectivity data at 0.5° elevation from the KLVX WSR-88D at 1405 (left), 1508 (middle), and 1635 UTC 15 Apr (right). Squall line motion is east at about 40 kt. Contours are at 10-dBZ intervals from 20 to 60 dBZ; values over 30 (50) dBZ are shaded light (dark). KY, IN, storm 1, and the 230-km (124 nmi) range ring from the radar (small +) are indicated.

difficult to assess whether shear and helicity values actually were greater over central Kentucky, as measured by the KLVX radar, than those computed from Paducah's sounding across western Kentucky. However, KLVX-derived shear values were approximately 5 m s^{-1} greater than that measured from the WSR-88D near St. Louis (KSLX) (Przybylinski et al. 1996), indicating an increased potential for mesocyclone development. Indeed, embedded bowing line segments and associated cyclonic circulations were more numerous over central Kentucky than earlier in the squall line's life cycle across Illinois and eastern Missouri.

3. Overall squall line evolution

Base reflectivity data between 1400 and 1700 UTC showed a serial-type (Johns and Hirt 1987) extensive squall line across Kentucky and Indiana with several bowing segments on the leading edge (Fig. 3). The mature line exhibited symmetric ''leading line-trailing stratiform'' structure (Houze et al. 1989). Along the length of the leading convective line, a persistent tight low-level reflectivity gradient signified the presence of strong, low-level convergence and ascent, resulting in the development of intense multicellular convection. Individual cells then merged very quickly with the squall line as it moved east at approximately 20 m s^{-1}. Immediately behind the leading line existed the so-called transition zone, wherein precipitation intensity was a relative minimum. Significant ''stratiform'' rainfall existed behind the transition zone during the mature stage of the squall line (Fig. 3), signifying the presence of moist storm-relative front-to-rear flow at higher altitudes within the anvil portion of the MCS (e.g., Houze et al. 1989). The presence of this trailing rainfall along with several bowing segments along the leading convective line suggested the existence of well-established local enhancements of the RIJ.

Across central Kentucky and south-central Indiana, a total of seven coherent and trackable bowing segments (referred to here as *storms*) were identified along the leading squall line, each segment associated with at least one rotational cyclonic circulation near its bow apex (Fig. 4). Two other bowing segments existed as well, although definitive, trackable circulations were not evident. Storms 1, 2, and 3 (Fig. 4) were relatively long lived (well over 1 h), averaged 25–40 km in length, and exhibited multiple rotational circulations. These segments produced several tornadoes of F0–F2 intensity and considerable downburst straight-line wind damage along or near their bow apexes. In contrast, storms 4, 5, 6, and 7 were shorter lived (less than 60 min), averaged 20–30 km in length, and each contained only a single identifiable cyclonic vortex. These segments apparently produced no tornadoes, although straight-line wind damage occurred along each storm's bow apex. Finally, storm 8 (Fig. 4) was an isolated cell immediately ahead of the squall line that then merged with the line. The storm produced a short-lived, weak tornado (F0 damage) over east-central Kentucky.

4. Structure and evolution of storm 1

a. Characteristics of storm 1, circulations 1–4

Storm 1 was, by far, the most intense, long-lived, and complex bowing line segment observed across central Kentucky and south-central Indiana on 15 April. KLVX WSR-88D low-level base velocity data (not shown) revealed that storm 1 was associated with a locally enhanced section of the RIJ, directed nearly normal to the major axis of the squall line. The bowing segment was observed on the KLVX radar for approximately 4 h, in which time it exhibited both multicellular and supercellular-like characteristics and multiple cyclonic circulations. During this period, the radar was able to iden-

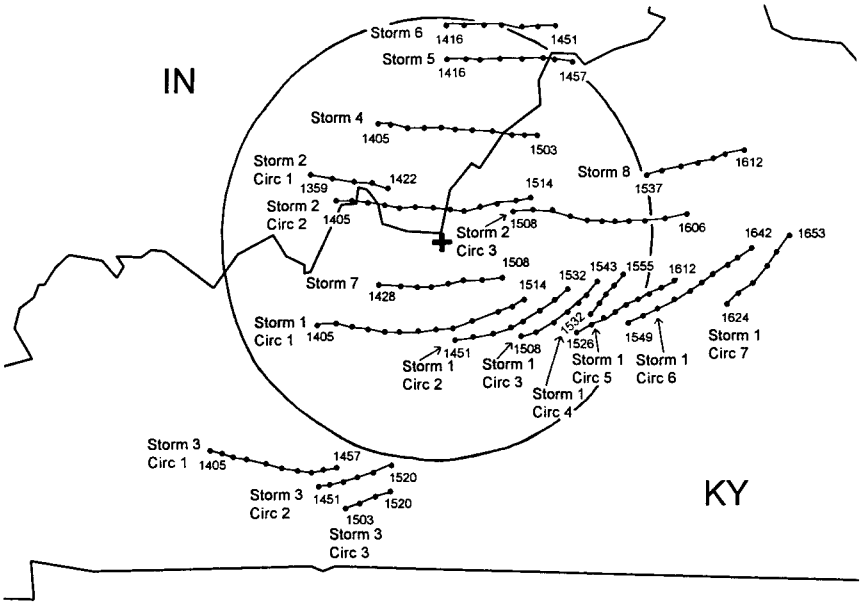

FIG. 4. Rotational cyclonic circulation (Circ) tracks identified for each bowing line segment (storm). Black dots along the tracks represent 5–6-min interval circulation locations with beginning and ending times (in UTC) indicated. The 100-km (54 nmi) range ring from the KLVX WSR-88D (+ sign) is shown.

tify seven coherent circulations between 1405 and 1653 UTC across central Kentucky along or near the leading edge of the storm segment (Fig. 4).

Circulation 1 (Fig. 4) first was detected at 1405 UTC along the bow apex of storm 1. The vortex fluctuated in intensity between 1405 and 1422 UTC, then displayed a definitive increase in rotational velocity (V_r) values [up to 23 m s^{-1} (45 kt)] thereafter (Fig. 5), while maintaining a 2–4-km diameter in the low levels. Limited radar viewing angles prevented circulation resolution above 3 km during its mature stage. During its maximum intensity, circulation 1 (45–55 km from the radar) met the V_r criteria associated with a moderate-to-strong mesocyclone (Burgess et al. 1993; Burgess and Lemon 1990) and produced F1–F2 tornado damage coincident with peak mesocyclone strength. Significant straight-line wind damage also occurred along the bow apex.

Circulation 1 weakened and broadened after 1503 UTC (Fig. 5), as circulation 2 (Fig. 4) quickly strengthened immediately south of the first vortex. The second vortex also produced a transient tornado with F1 damage as 0–3-km V_r values (not shown) ranged from 18 to 23 m s^{-1} (35–45 kt). Circulation 2 initially was detected at low levels (0.5–2.5-km altitude) along the bow apex, strengthened just prior to tornado occurrence, then weakened and broadened by 1532 UTC as it propagated rearward with respect to the apex. The rearward convective cell propagation (and gradual vortex weakening) relative to the leading line resulted from cell motion that was slower than the overall motion of the squall line (about 20 m s^{-1}).

Circulations 3 and 4 (Fig. 4) also developed as definitive low-level cyclonic-convergent zones along the bow apex, intensified and deepened upward, then eventually broadened and became less defined as they propagated rearward compared to the leading line. Detailed reflectivity and storm-relative velocity map (SRM) data analyses revealed that four separate circulations (2–5) apparently existed simultaneously at different life cycle stages within a larger low-to-middle-level cyclonic ''swirl'' region (e.g., at 1532 UTC in Fig. 6) associated with storm 1. The swirl region, defined by storm-relative rear-to-front flow along and behind the leading bow apex and enhanced front-to-rear flow ahead and north of the apex, persisted during much of storm 1's mature stage. In organized, long-lived bowing segments such as storm 1, the observation of persistent overall swirl or shear regions may suggest significant convergence between the RIJ and storm-relative inflow ahead of the line. This may promote multiple vortex development along/near the low-level bow apex (gust front) with subsequent intensification through vertical stretching in the updraft. Multiple cyclonic vortex evolution within a swirl region also was noted in an organized, tornado-producing bowing squall line studied by DeWald et al. (1998).

The multiple core vortex evolution observed in storm 1 appears similar to that documented by Burgess et al. (1982), in that a temporal overlap occurred between the organizing stage of new cores and the dissipating stage of older ones. In storm 1, multiple (2–4) circulations existed simultaneously, with up to 10–20-min periods of overlap between successive vortices. It is interesting to note that storm 1, circulation 1 had relatively long

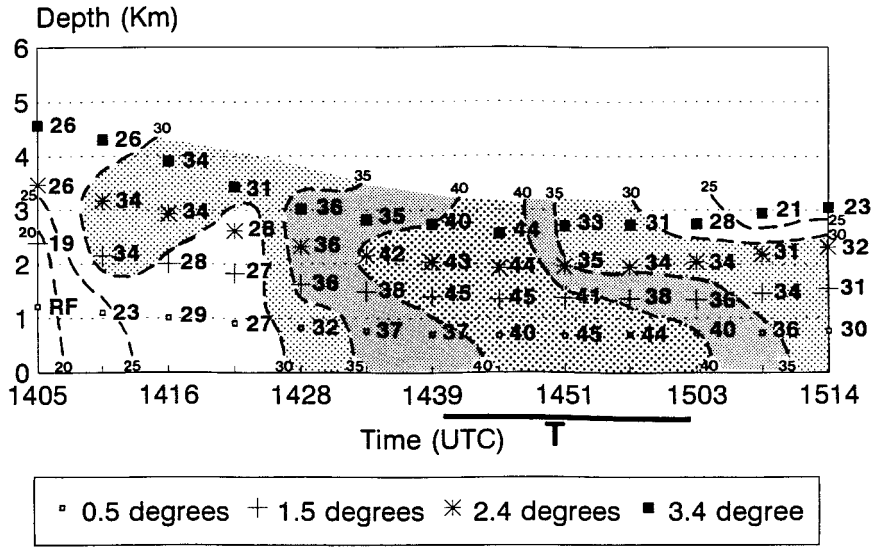

FIG. 5. Magnitudes of rotational velocity (V_r in kt) for storm 1, circulation 1 at 0.5°, 1.5°, 2.4°, and 3.4° radar elevation. Values over 30 kt are shaded. Time in UTC and radar-indicated depth (altitude) in km are shown. The T and adjacent straight line reveal the period of a tornado associated with the circulation. The RF at 1405 UTC denotes range-folded data.

organizing and mature stages (Figs. 4 and 5), while subsequent cores (circulations 2–4) evolved more quickly. This core life cycle trend appears analogous to that noted by Burgess et al. (1993) for multiple mesocyclone cores associated with supercells.

b. Development of HP supercell-like characteristics (circulation 5)

Circulation 5 initially was identified as a relatively weak low-level cyclonic-convergent area associated with new convective growth along storm 1's bow apex at 1526 and 1532 UTC (Fig. 6). The convection intensified rapidly between 1537 and 1600 UTC (Fig. 7), accompanied by a corresponding substantial increase in the strength and vertical depth of circulation 5 (Fig. 8). The evolution of this cyclonic updraft rotation resulted in a redistribution of the heaviest precipitation and the appearance of HP supercell-like characteristics within storm 1.

Specifically, by 1600 UTC, a low-level forward flank weak-echo region (WER) clearly was evident, indicative of a pronounced inflow and updraft zone within the complex, along with an elevated maximum reflectivity core, subtle bounded weak-echo region (BWER), and downshear echo overhang aloft (Fig. 9). The elevated BWER, marked by 40–50-dB*Z* reflectivity values surrounded by values of 55–65 dB*Z*, was identifiable from 1549 to 1606 UTC. Corresponding storm-relative velocity data at 1600 UTC showed a well-defined, deep-layered (above 7 km) cyclonic vortex (Fig. 10) coincident with the low-level WER and middle-level BWER (Fig. 9). At its peak, circulation 5 (Fig. 8) met supercell mesocyclone depth and strength criteria [e.g., approximately 20 m s^{-1} (40 kt) V_r from 3- to 7-km altitude at 1600 UTC as measured 90–100 km east of the KLVX WSR-88D]. It should be noted that although reflectivity values within the low-level WER were relatively low compared to the storm's maximum reflectivity core, measured values ranged from 30 to 40 dB*Z*. In other words, the mesocyclone was embedded within precipitation, which is characteristic of HP storms (Doswell and Burgess 1993). Circulation 5 resulted in a tornado that produced F1 damage from about 1548 to 1602 UTC (*T* in Fig. 8), coincident with vortex intensification and deepening, and the appearance of HP supercell-like characteristics.

The apparent diameter of the mesocyclone remained narrow during its low-level organizing stage, with roughly a 1–2-km diameter between 1532 and 1543 UTC (Fig. 11). The sampled vortex then broadened slightly (2–4-km diameter) as it strengthened and matured between 1543 and 1600 UTC. After 1606 UTC, HP stormlike reflectivity characteristics quickly became less pronounced (Fig. 7), associated V_r values decreased (Fig. 8), and the circulation's diameter broadened to 4–7 km (Fig. 11). However, a rapid transition occurred to a comma head–comma tail pattern.

c. Transition to a bow echo with a rotating comma head–comma tail (circulations 6 and 7); radar sampling issues

The southern flank of the HP storm's reflectivity pattern transitioned to a distinctive bow echo after 1606 UTC, with a rotating comma head and comma tail (Fig. 7). Przybylinski (1995), Moller et al. (1994), and Doswell et al. (1990) have documented this type of tran-

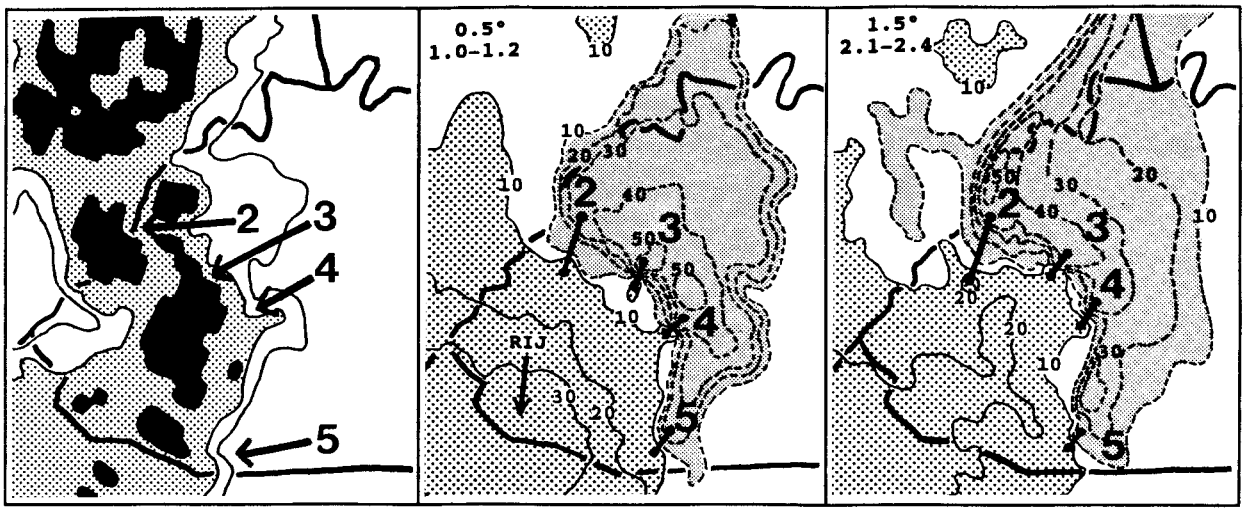

FIG. 6. Base reflectivity at 0.5° and SRM data at 0.5° (1.0–1.2 km) and 1.5° (2.1–2.4 km) elevation at 1532 UTC. Reflectivity data are contoured every 10 dBZ starting at 30 dBZ; values greater than 40 (50) dBZ are shaded light (dark). SRM data are contoured every 10 kt; the zero isodop is not drawn for clarity purposes. A cyclonic swirl area is evident in SRM data with dashed/gray-shaded (solid/dot-shaded) contours denoting storm-relative inbound (outbound) radial winds (in kt) with respect to the radar located 65–75 km west (left) of the area shown. Within the swirl zone, four cyclonic vortices (circulations 2–5) associated with convective cells are identified by numbers and short, bold straight lines. RIJ denotes an elevated rear-inflow jet. A bold county overlay is provided for reference.

sition and stated that the bow echo may be a variation or evolutionary stage of the HP supercell family. The echo bulging, which caused considerable surface wind damage, was associated with a downburst/RIJ surge and the development of a pronounced weak echo channel (WEC in Fig. 7) after 1606 UTC just behind the intense reflectivity zone. Aloft, reflectivity data revealed that the comma structure possessed significantly higher echo tops (i.e., deeper convection) than adjacent portions of the squall line, likely due in part to the presence of a cyclonically rotating updraft (Fig. 12) within the comma region.

Shortly prior to the transition of the HP-like storm to a comma head–tail structure, a sixth low-level cyclonic-convergent zone (circulation 6) was identified along the gust front and nose of the RIJ. The incipient circulation was confined to the lower atmosphere (Fig. 12) until the transition occurred. After the transition, the vortex increased in strength and depth, especially between 1612 and 1624 UTC (Fig. 12), as it became enveloped within the southeast quadrant of the comma head structure (Fig. 13). Note that at 1624 UTC (Fig. 12), the circulation met mesocyclone V_r and depth criteria, with highest V_r values (25 m s^{-1}/50 kt) at about 4.5-km altitude (i.e., the 1.5° radar elevation angle). The circulation at 1.5° elevation was strong and ''gate to gate,'' but appeared weaker and slightly broader at 0.5° (Fig. 13). Given lower- and middle-level reflectivity and V_r trends, it is obvious that circulation 6 intensified between 1618 and 1624 UTC. However, given the considerably stronger and tighter vortex at 1.5° versus 0.5° elevation at 1624 UTC (Figs. 12 and 13), and the 9 m s^{-1}/18 kt increase in V_r at 1.5° in one volume scan (i.e., from 1618 to 1624 UTC) without a retrieved corresponding increase at 0.5° (Fig. 12), it also is possible that radar sampling may be partly responsible.

Specifically, the radar *aspect ratio* relates the diameter of a particular precipitation or flow field entity to the diameter of the radar beam, that is, the radar-illuminated volume (Burgess et al. 1993; Burgess and Lemon 1990). If a target is small compared to the radar volume (beamwidth), then the target either may be essentially undetectable or, more likely, improperly sampled by the radar. The effects of radar sampling were simulated by Wood (1996). In this case, it seems likely that at 1.5° elevation the radar beam centerline (maximum power) of two adjacent beams intercepted the maximum inbound and outbound radial components of the mesocyclone's solid-body rotation, resulting in the strong gate-to-gate shear shown in Fig. 13. At the same time, the appearance of the circulation at 0.5° (Fig. 13) suggests that the radar *may* not have sampled the mesocyclone core optimally, resulting in a slightly broader vortex and averaged V_r values that were lower than reality. Note that one volume scan later (1629 UTC), V_r values at 1.5° dropped rapidly from that at 1624 UTC, suggesting a weakening vortex (Fig. 12). However, one must consider whether this weakening represents a significant meteorological change or again is an artifact of improper radar sampling. It can be difficult to separate explicitly actual versus artificial convective trends, although accompanying reflectivity structure (Fig. 7) suggested that the circulation likely began weakening at least somewhat between 1624 and 1629 UTC. Improper target sampling at increasing range is an inherent problem with any radar, although the WSR-88D is less vul-

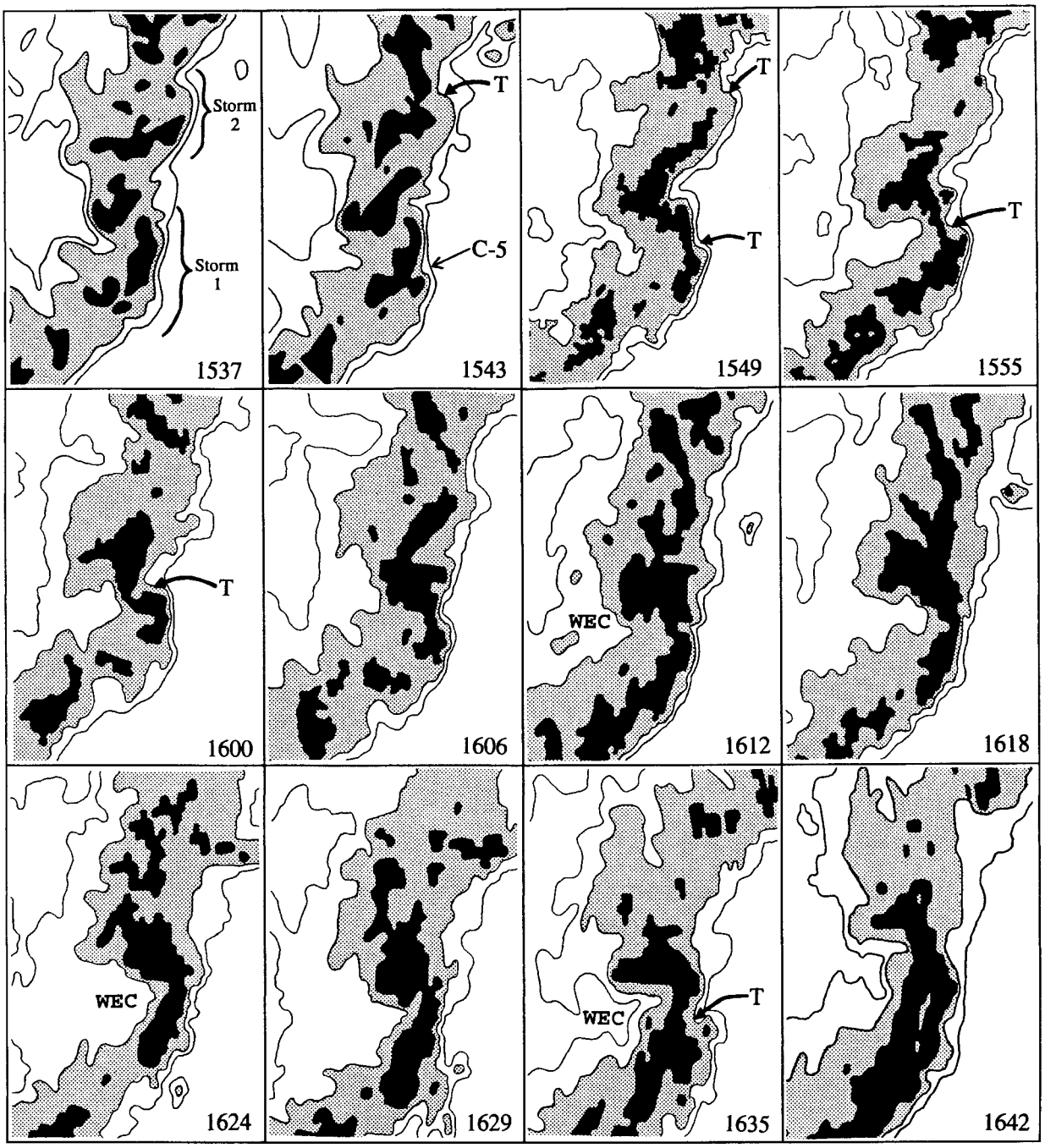

FIG. 7. Sequence of base reflectivity images at 0.5° elevation showing the evolution of storm 1 between 1537 and 1642 UTC. The latter stage of storm 2 also is indicated, but is no longer evident after 1606 UTC. The reflectivity contouring and shading scheme is identical to that in Fig. 6. The T denotes the locations of tornadoes, C-5 at 1543 UTC shows convection associated with circulation 5, and WEC identifies weak-echo channels behind the leading convective line (WEC is not shown on all panels).

nerable than previous radars that possessed larger beamwidths. Nevertheless, forecasters must be aware of potential sampling problems and incorporate this knowledge into their data analyses so that proper warning decisions can be made. Accompanying reflectivity structure and access to data from adjacent radar sites are crucial in evaluating sampled trends in distant mesocyclone evolution. In addition, Sohl et al. (1996) presented a basic radar selection methodology to help forecasters contend with sampling issues.

Although surface wind damage was associated with circulation 6, no tornadoes could be confirmed. How-

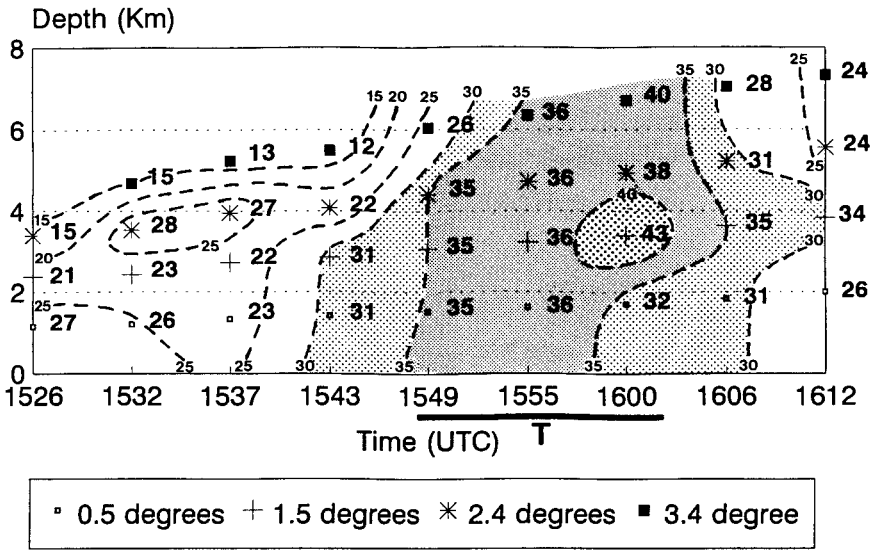

FIG. 8. Same as Fig. 5 except V_r for storm 1, circulation 5.

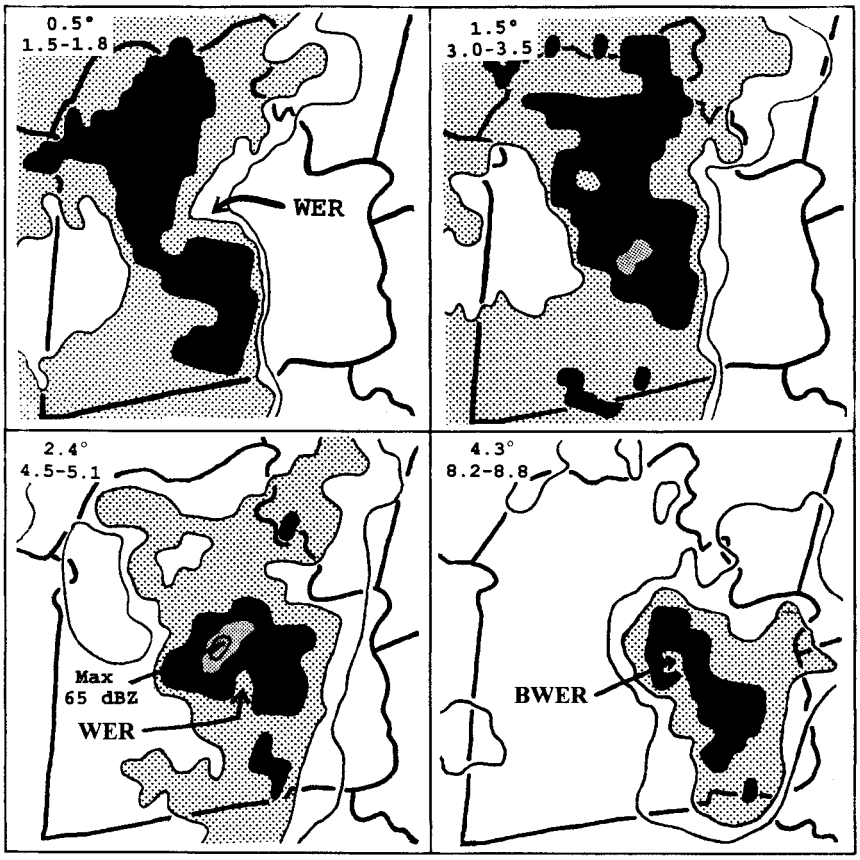

FIG. 9. Base reflectivity data at 1600 UTC showing the vertical characteristics of the HP supercell-like structure embedded within storm 1. The radar elevation angle (top number) and approximate beam height (bottom numbers in km) are indicated in the upper-left corner of each panel. The reflectivity contouring and shading scheme is identical to that in Fig. 6; values over 60 dBZ are lightly shaded inside the dark 50-dBZ area. WER denotes a weak-echo region; BWER identifies a bounded WER. A bold county overlay is provided for reference purposes to view storm tilt.

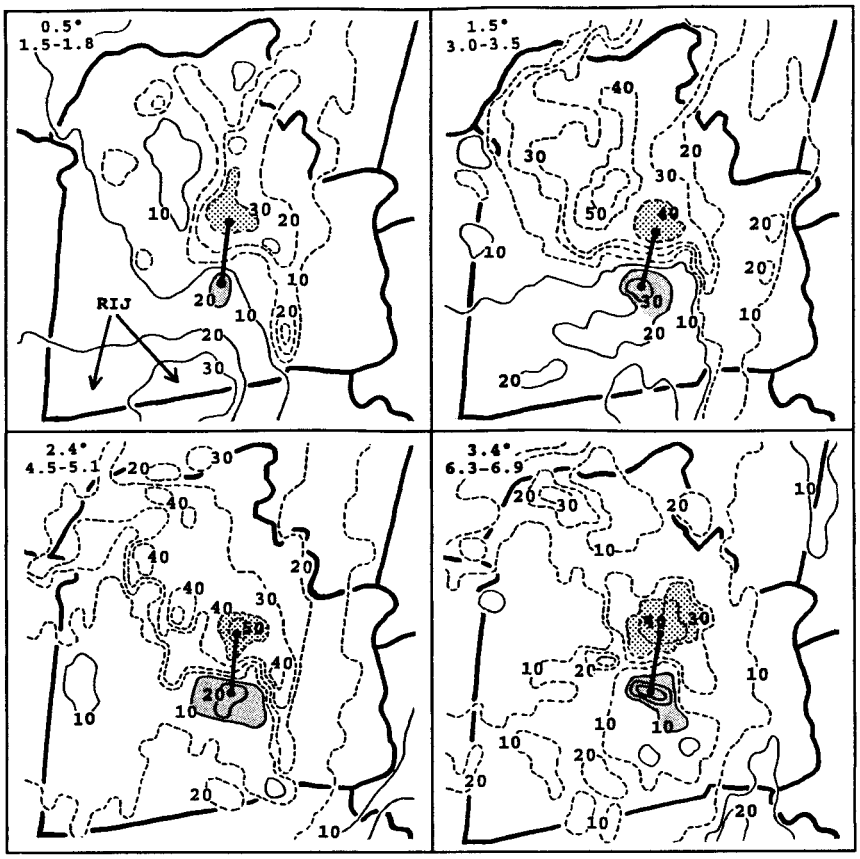

FIG. 10. SRM data at 1600 UTC showing the vertical characteristics of the mesocyclone associated with the HP supercell-like structure within storm 1. The radar elevation angle and approximate beam height (in km) are indicated in each panel. Dashed/dot-shaded (solid/gray-shaded) contours denote inbound (outbound) radial winds with respect to the radar located 90–100 km west (left) of the area shown. Only maximum winds associated with the mesocyclone (circulation 5) are shaded; a bold solid line defines the core.

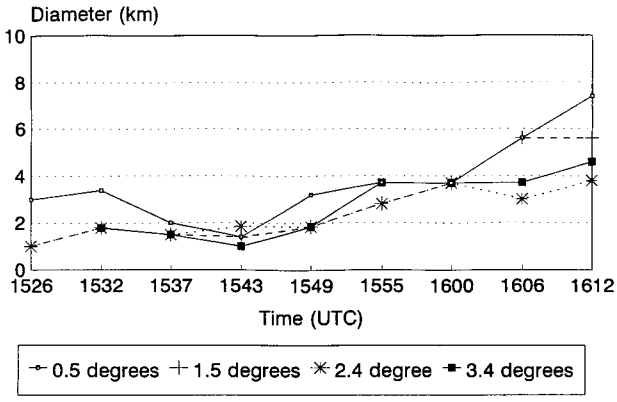

FIG. 11. Mesocyclone diameter (in km) vs time (in UTC) associated with storm 1, circulation 5 at 0.5°, 1.5°, 2.4°, and 3.4° radar elevation.

ever, the position of the vortex during its mature stage, that is, in the southeast quadrant of the comma head just north of the bow apex (Fig. 13), represents a location where tornadoes can occur (Przybylinski 1995). In fact, local National Weather Service verification of several similar events in recent years across central Kentucky and southern Indiana have confirmed tornadoes of F0–F2 intensity in the same relative location as that shown in Fig. 13.

As circulation 6 weakened and broadened after 1624 UTC within the comma head, a new vortex (circulation 7) quickly developed along the comma tail (track shown in Fig. 4). Similar to earlier vortices, circulation 7 was noted initially along the low-level bow apex, followed by deepening and intensification (Fig. 14) as it propagated northeastward with respect to the eastward-moving squall line. The vortex produced a tornado with F0 damage between 1630 and 1640 UTC (T at 1635 UTC in Fig. 7) as highest detected V_r values remained in the lower atmosphere (Fig. 14). Given lower detected rotational velocity values at higher altitudes and the cir-

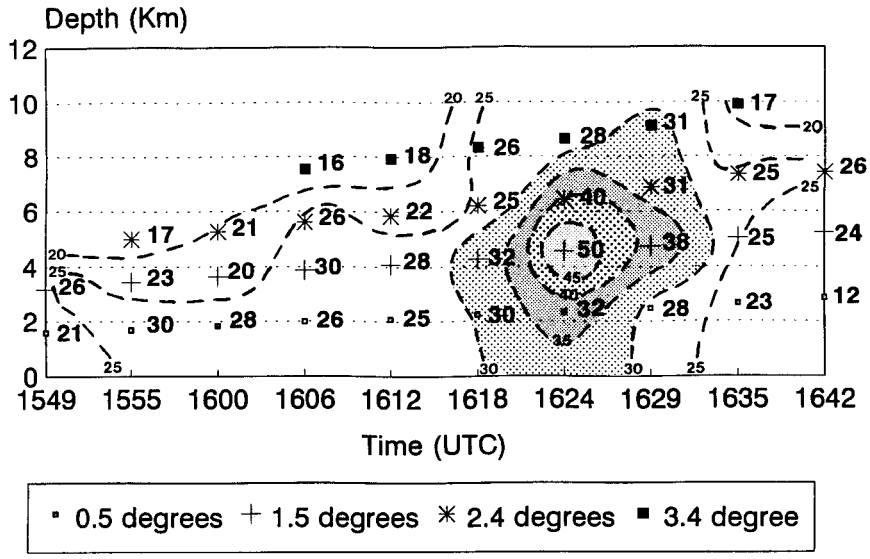

FIG. 12. Same as Fig. 5 except V_r for storm 1, circulation 6.

culation's distance from the radar (140–145 km), it is possible that the circulation was stronger than detected due to aspect ratio concerns, and that the highest V_r values were below the radar's lowest viewing volume.

In summary, storm 1 exhibited HP supercellular characteristics within an essentially multicellular convective complex, an evolution that Doswell and Burgess (1993) note can occur. As is common, the HP-like storm in this case apparently evolved from convective-scale processes within a strongly forced portion of the squall line and possibly local changes in the environmental shear profile. It then evolved into a distinct bow echo with a rotating comma head and comma tail. Storm 1's HP and subsequent bow echo stages contained multicellular elements, as three separate circulations (5–7) were associated with the complex. Moller et al. (1994) and Nelson (1987) have termed similar cases *multicell–supercell hybrids* that may belong to the supercell family.

d. Bookend vortices within storm 1

Weisman (1993) discussed the development and role of cyclonic and anticyclonic bookend vortices along the edges of simulated bow echoes. He suggested that these vortices develop as a result of upward tilting and stretching of horizontal vorticity within a sheared environment, followed by downward tilting within the downdraft. Bookend or line-end vortices typically are located on

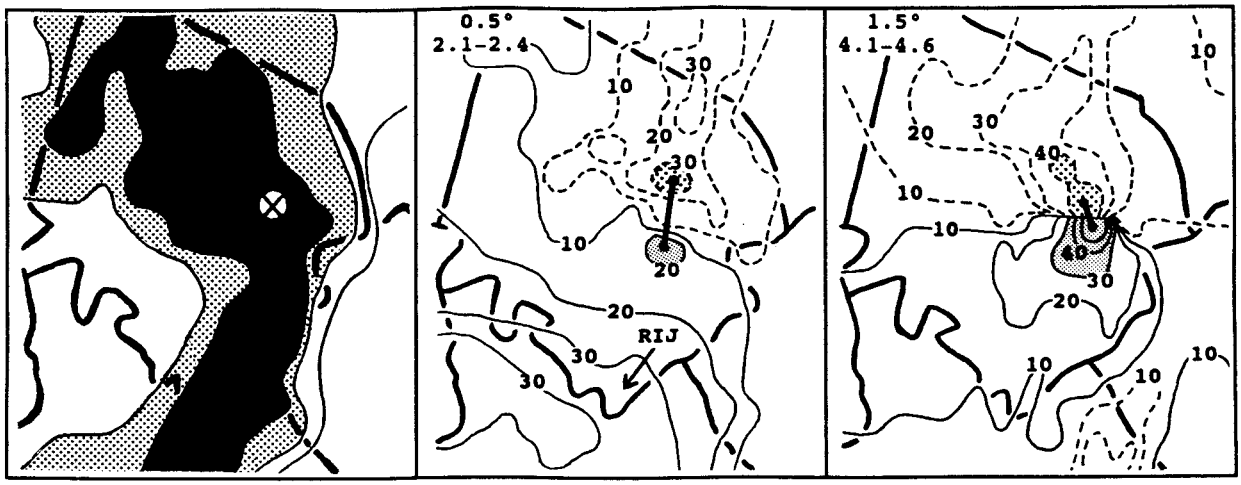

FIG. 13. Reflectivity data at 0.5° elevation and SRM data at 0.5° (2.1–2.4 km; middle) and 1.5° (4.1–4.6 km; right) elevation at 1624 UTC. The reflectivity (SRM) contouring and shading scheme is the same as that in Fig. 6 (Fig. 10). The radar is located 120–125 km west (left) of the area shown. The × within the unshaded circle on reflectivity data reveals the location of circulation 6 with respect to reflectivity structure. On SRM data, circulation 6's maximum inbound and outbound winds are shaded and connected by a bold solid line.

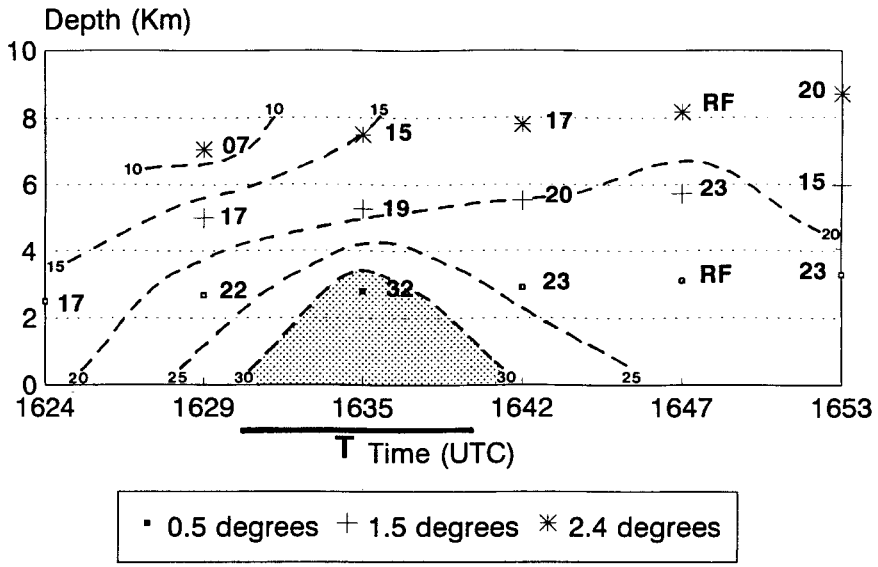

FIG. 14. Same as Fig. 5 except V_r for storm 1, circulation 7.

the edges of and remain close to leading convective line segments in strongly sheared environments, and tend to enhance the rear-inflow jet to promote continued deep convective growth and increased longevity of bow echoes (COMET 1997). Funk et al. (1996b) and Przybylinski and Schmocker (1993) noted possible bookend vortices for two bow echo–producing MCSs over Missouri. However, documentation showing the presence of these vortices using WSR-88D data and their generation and evolution processes within complex squall lines apparently still is limited.

The evolution of storm 1 appears consistent with Weisman's (1993) idealized bow echoes, which contained bookend vortices. Specifically, storm 1 was associated with a well-developed rear-inflow jet, multicellular convection, numerous rotational cyclonic circulations, and enhanced trailing stratiform precipitation. In addition, KLVX WSR-88D data showed the presence of middle-level strong shear (swirl) zones, as evident in a sequence of reflectivity (Fig. 15) and storm-relative velocity images (Fig. 16) from 1520 to 1618 UTC. Persistent channeled rear-to-front (i.e., left to right) flow was present (Fig. 16), coincident with a notable WEC in reflectivity data (Fig. 15). Surrounding the rear-to-front airstream were areas of front-to-rear flow on the north and south peripheries of the bowing structure (Figs. 15 and 16), a distance (diameter) of 15–25 km. The data seem consistent with the findings of Weisman (1993) and COMET (1997), suggesting that bookend/line-end vortexlike structures were present (e.g., as shown by the bold arrows at 1543 UTC in Fig. 16), which promoted continued new growth of intense leading line convection along the bow apex of storm 1 (Fig. 15). Note that the front-to-rear flow within the cyclonic shear zone was strong and associated with a significant westward (upwind) extension of the 50–60-dBZ area, while the weaker anticyclonic side frequently was coincident with a subtle upwind extension of 50-dBZ returns. Mature updraft circulations associated with storm 1 generally were located just poleward and downwind of the rear inflow and bookend vortexlike structures before broadening and becoming less defined within the overall cyclonic swirl zone.

e. Midaltitude radial convergence

Several researchers have studied convergence zones within convective storms to determine their effect on severe weather phenomena. For example, Lemon and Parker (1996) and Lemon and Burgess (1992) documented the existence of a *deep convergence zone* (DCZ) within supercell storms. The DCZ was coincident with the gust front at low levels and extended upward to an average depth of 10 km. Mesocyclones, tornadoes, and damaging winds occurred along or near the narrow zone of intense convergence. Eilts et al. (1996) investigated over 85 microburst-producing pulse thunderstorms and determined that deep convergence in their middle levels was one of the most effective radar precursors to surface wind damage. Przybylinski et al. (1995), Schmocker et al. (1996), and Funk et al. (1998) studied the storm-relative midaltitude radial convergence (MARC) signature to determine its utility in predicting the onset of damaging downburst surface winds associated with squall lines and bow echoes. Their findings suggested that MARC values (i.e., the radial velocity differential) of 25–30 m s^{-1} or more at 3–7-km altitude were noted *before* significant bowing occurred at low levels, and that maximum MARC preceded the occurrence of damaging surface winds by 10–20 min.

Within storm 1, moderate-to-strong midaltitude con-

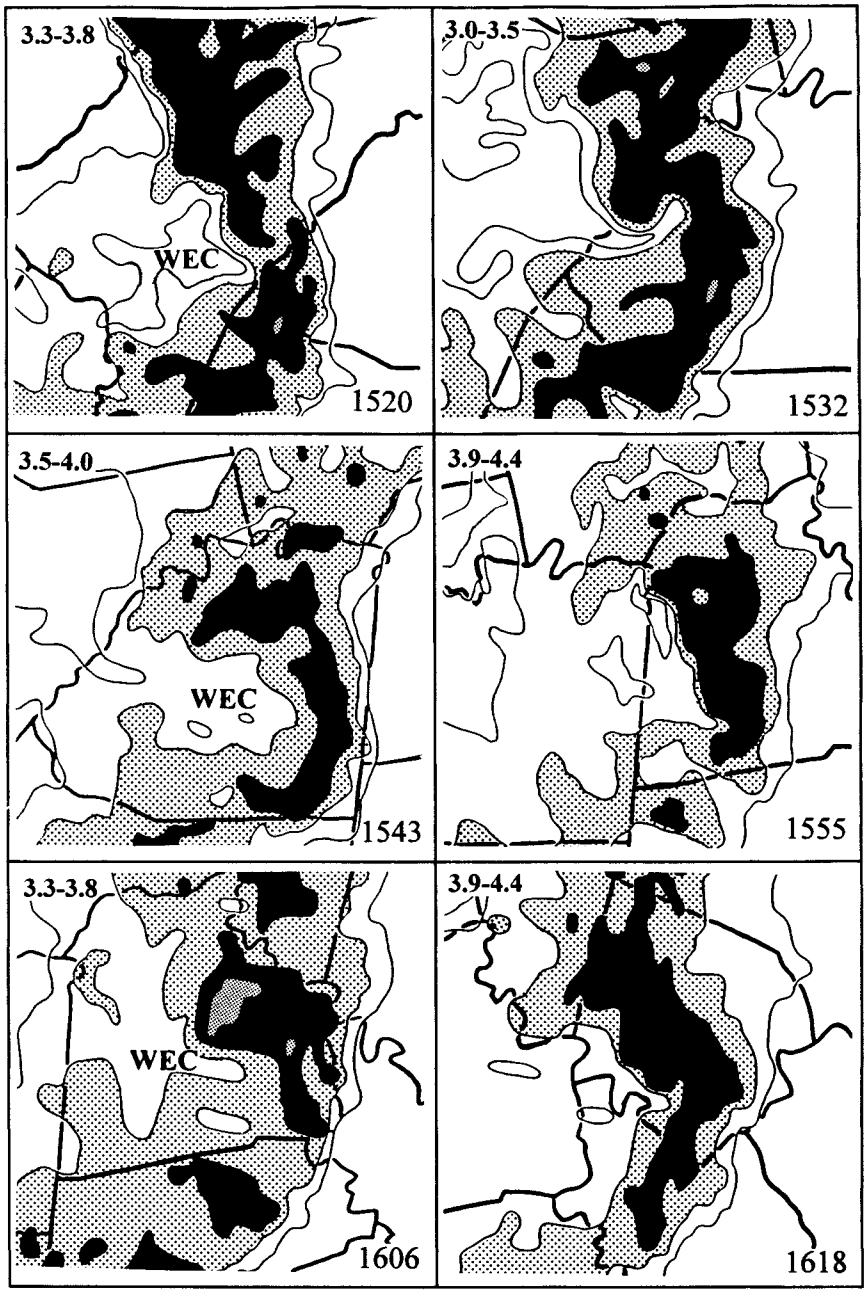

FIG. 15. Reflectivity data from 1520 to 1618 UTC (every other volume scan). The approximate range in height (in km) of the data shown is indicated in the upper-left corner of each panel (an attempt was made to keep the data at similar heights using different radar elevation angles as necessary). The reflectivity contouring and shading scheme is identical to that in Figs. 6 and 9. WEC is present on all panels shown but only labeled on every other panel. The KLVX radar is located about 50 km west-northwest (left) of the center point of the 1520 UTC panel and about 115 km from the center of the 1618 UTC panel.

vergence was noted after 1500 UTC; it generally was less apparent before 1500 UTC due in part to an unfavorable radar viewing angle of the signature. Retrieved values of MARC ranged from 23 to 30 m s^{-1} between 1500 and 1600 UTC; retrieved values then decreased to 15–20 m s^{-1} by 1630 UTC. The convergence generally was noted along storm 1's leading bow apex at altitudes ranging from 3.5 to 6 km. For example, at 1543 UTC, convergence values were at least 25 m s^{-1} at nearly 4-km altitude along the front flank of the convective system (M in Fig. 16). The high values and altitude of MARC within storm 1 were consistent with

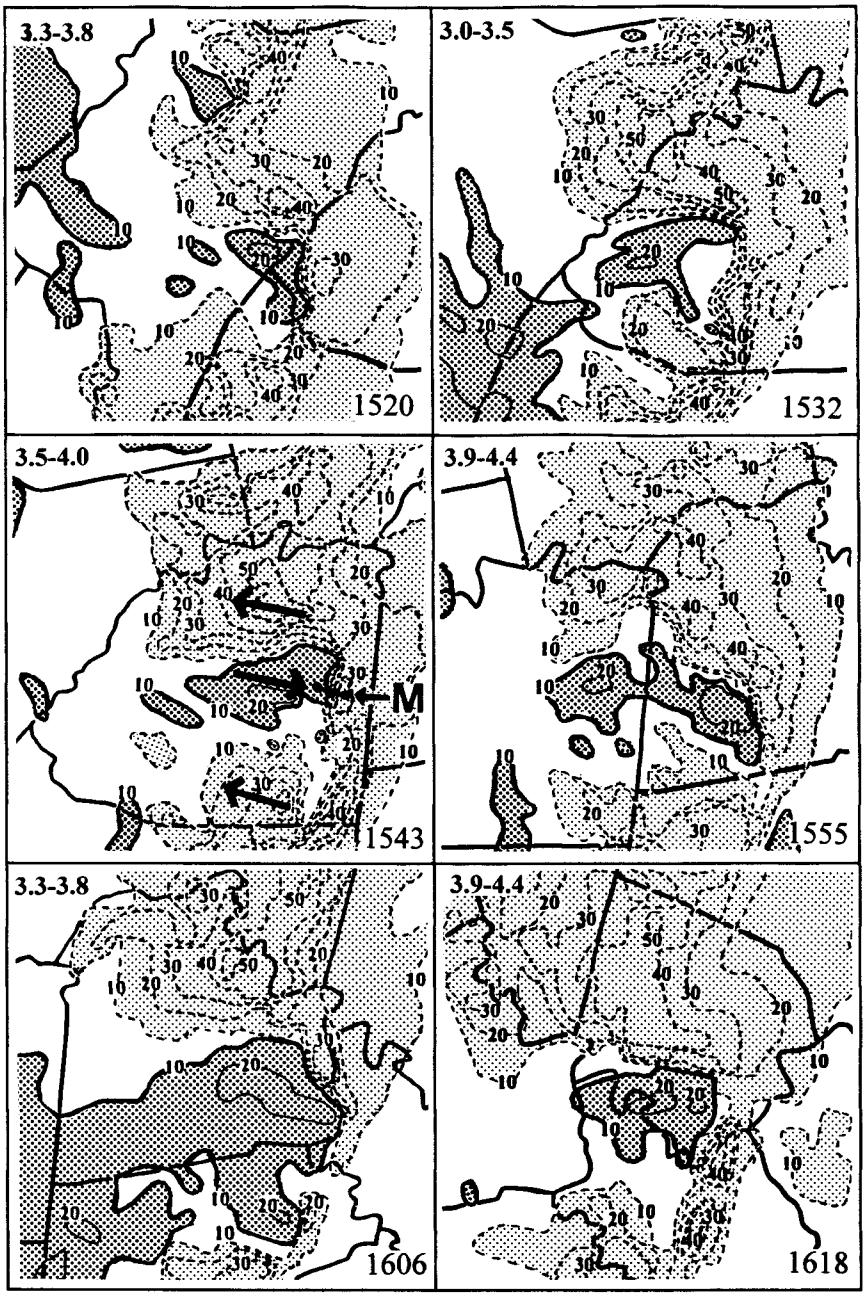

FIG. 16. Corresponding SRM data (in kt) from 1520 to 1618 UTC (every other volume scan) to match the reflectivity data shown in Fig. 15. The lighter (darker) shading represents storm-relative radial winds directed toward (away from) (e.g., as shown by bold arrows at 1543 UTC) the radar site located to the west-northwest of the area shown. The letter M at 1543 UTC points toward a zone of MARC.

that shown by Schmocker et al. (1996) and Funk et al. (1998); however, damaging downbursts from storm 1 already were ongoing prior to the identification of MARC. Therefore, the convergence may have signified that damaging surface winds would continue downstream along the path of the bowing line segment. Coherent MARC was not as readily detectable within other bowing line segments (storms) in this study.

5. Structure and evolution of other storms

a. Evolution of storms 2 and 3

The evolution of storms 2 and 3 appeared less organized and complex than that of storm 1. Nevertheless, each bowing line segment produced multiple cyclonic circulations, albeit fewer than storm 1. Storm 2 (identified at 1537 UTC in Fig. 7), which moved from south-

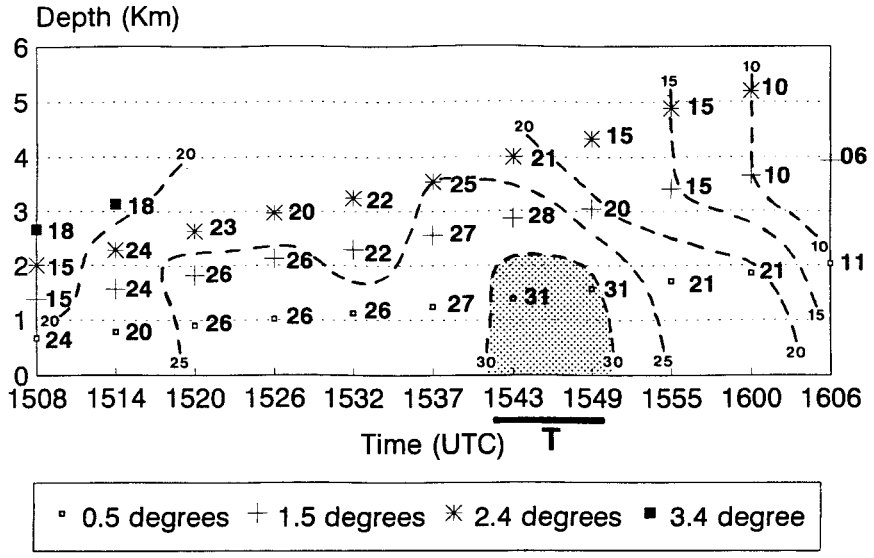

FIG. 17. Same as Fig. 5 except V_r for storm 2, circulation 3.

central Indiana to east-central Kentucky, contained three identifiable circulations (Fig. 4), each located along or just north of the bow apex. The first two circulations produced no tornadoes, although a path of significant straight-line wind damage was highly correlated to the location of the bow apex. Circulation 3, on the other hand, produced a tornado with F0 damage from approximately 1542 to 1550 UTC (T at 1543 and 1549 UTC in Fig. 7), coincident with a modest low-level increase in V_r values as measured 85 km from the radar (Fig. 17). It is interesting to note that circulations associated with storm 2, including the tornado-producing vortex, developed in and remained confined mainly to the lower levels of the atmosphere, a finding similar to that documented by Wakimoto and Wilson (1989).

Storm 3, a bowing segment located 120–140 km from the radar across south-central Kentucky, produced three cyclonic circulations along or near the bow apex (Fig. 4). Of the three, circulation 2 produced F1 tornadic damage in the city of Bowling Green, with significant straight-line winds and 1-in.-diameter hail reported just south of the tornado. This pattern is very similar to that documented by Forbes and Wakimoto (1983), in that tornadic damage occurred just north of maximum straight-line or microburst wind damage. The pattern also is consistent with Przybylinski's (1995) finding that tornadoes associated with bowing line segments typically occur just north of the apex of the bow. Similar to storm 2, circulation 3 (Fig. 17), the V_r trace for storm 3, circulation 2 (Fig. 18) revealed a modest increase in vortex strength just prior to tornado touchdown, highest V_r values during the tornado, and weakening thereafter. Moreover, highest V_r values again were confined to the low levels similar to that noted by Wakimoto and Wilson (1989). Given the distance of the circulation from the radar site and the fact that the vortex was being sampled nearly orthogonal to the movement of the storm, retrieved V_r values as shown in Fig. 18 may be lower than actual values within circulation 2. Despite this, vortex trends appeared valid and correlated well to observed severe weather phenomena.

b. Evolution of storms 4–7

The other bowing line segments observed within the 15 April squall line (i.e., storms 4–7; Fig. 4) generally were smaller scale, shorter lived, and at times more subtle in appearance in reflectivity data than were storms 1–3. Despite this subtlety, storms 4–7 generated wind damage in several areas. Each segment produced only one identifiable rotational cyclonic circulation, often to an altitude of 4–5 km, although highest V_r values (not shown) were confined to the lowest 1–3 km of the atmosphere. None of the vortices could be correlated definitively to tornadoes, although measured V_r values periodically were similar to those circulations within storms 1–3 that did produce tornadoes.

6. Summary and conclusions

The 15 April 1994 squall line exhibited leading line–trailing stratiform symmetric structure over Kentucky and southern Indiana, and occurred within a dynamic, cool season environment consisting of strong wind shear and moderate instability. The squall line contained seven bowing segments with viewable circulations, which correlated highly to extensive straight-line wind damage and several tornadoes. Storm 1 was the most long-lived and complicated bowing segment in this study, and featured a persistent locally enhanced rear-inflow jet, a complex multicell/HP supercell-like evolution, and seven separate circulations. Each storm 1 circulation gen-

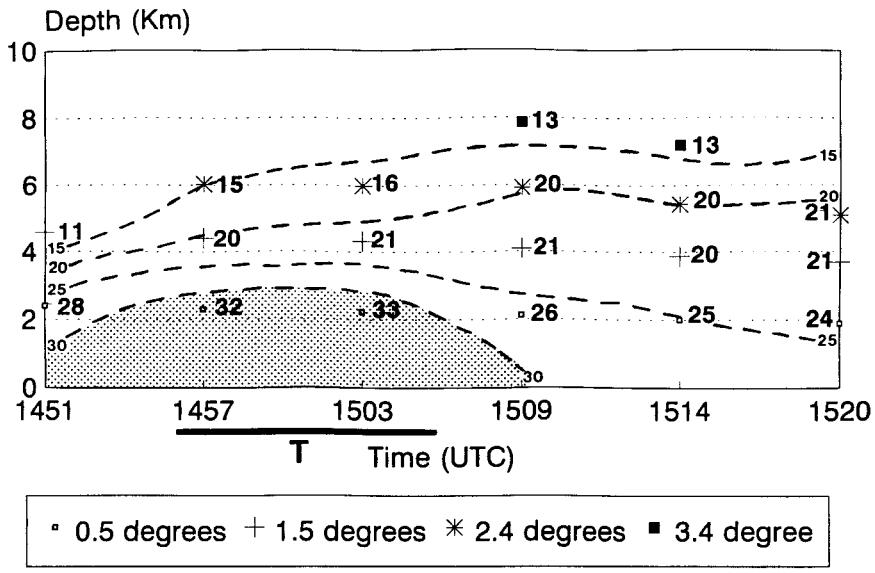

FIG. 18. Same as Fig. 5 except V_r for storm 3, circulation 2.

erally evolved in a similar cyclic fashion. Vortex genesis usually occurred as a low-level cyclonic-convergent area along the leading edge of the bow apex. Maturity was achieved through subsequent vortex strengthening and deepening while propagating poleward (northward) with respect to the apex. Dissipation included vortex broadening with a tendency for rearward line-relative propagation as new convective cells and low-level circulations initiated along the leading bow apex. Multiple circulations existed simultaneously at different stages of development within storm 1, some of which satisfied mesocyclone criteria during their mature stage. Tornadoes were highly correlated with low- and middle-level vortex intensification and deepening.

Storms 2 and 3 also exhibited multiple vortices, although they generally did not meet mesocyclone criteria as highest rotational velocity values were confined to the lowest few kilometers of the atmosphere. Nevertheless, storms 2 and 3 each produced at least one transient tornado. Storms 4–7 contained only one identifiable vortex apiece, each associated with straight-line wind damage but no tornadoes.

Several circulations identified by the KLVX WSR-88D on 15 April appeared similar to those in Wakimoto and Wilson (1989) in that shearing instabilities and convergence along the gust front apparently promoted low-level vortex genesis, followed by vortex intensification through vertical stretching within the convective updraft. Some storm 1 circulations, however, appeared more intense with a larger vertical depth than in their study due to stronger local convergence, shear, and forcing associated with a well-organized bowing segment.

The 15 April 1994 event illustrates the ability of the WSR-88D to detect some of the complex storm-scale interactions that can occur within severe squall lines. Forecasters have an excellent tool to assess severe weather potential, although a high degree of skill is critical for accurate and timely warning purposes, especially for rapidly moving squall lines with embedded bow echoes and tornadoes. Within such events, it seems reasonable to assume that radar operators might focus their greatest attention on the most prominent, identifiable features and less on subtle signatures. Indeed, in the 15 April case, storm 1 was the most distinct bow echo and produced the greatest amount of wind damage and tornadoes. However, as demonstrated here, severe weather is possible from more subtle bowing segments as well. Thus, forecasters might tend to issue *blanket warnings* for a fast-moving squall line, which at times may be the most feasible plan of action. However, the WSR-88D allows for better differentiation between the potential severity of convective cells. Forecasters should concentrate on reflectivity structure to locate bowing line segments, distinct or subtle, and typical locations of cyclonic circulations and tornadoes with respect to these segments. Vortex strengthening and deepening trends, especially for organized line segments containing multiple vortices, and the effects of radar sampling also must be monitored closely. This basic strategy will promote proper warning decisions and the ability to better define the degree of damage potential from severe storms.

Acknowledgments. The authors thank Mr. Marvin Maddox, meteorologist-in-charge (MIC), NWSFO Louisville; Mr. Dick Elder, MIC, NWSO Wichita; and Dr. Richard Livingston, chief, NWS Central Region Scientific Services Division for their support during this study. The authors also thank Mr. Bill Wilson, Office of Hydrology/Weather Service Headquarters, for archiving the KLVX WSR-88D radar data for this event, and two anonymous reviewers for their helpful com-

ments. Research has been conducted as part of a Cooperative Program for Operational Meteorology Education and Training Cooperative Project between Saint Louis University and the National Weather Service Forecast Offices in Louisville and St. Louis. This paper is funded from a subaward under a cooperative agreement between the National Oceanic and Atmospheric Administration (NOAA) and the University Corporation for Atmospheric Research (UCAR). The views expressed herein are those of the authors and do not necessarily reflect the views of NOAA, its subagencies, or UCAR.

REFERENCES

Burgess, D. W., and L. R. Lemon, 1990: Severe thunderstorm detection by radar. *Radar in Meteorology,* D. Atlas, Ed., Amer. Meteor. Soc., 619–647.

——, and B. F. Smull, 1990: Doppler radar observations of a bow echo associated with a long-track severe windstorm. Preprints, *16th Conf. on Severe Local Storms,* Kananaskis Park, AB, Canada, Amer. Meteor. Soc., 203–208.

——, V. T. Wood, and R. A. Brown, 1982: Mesocyclone evolution statistics. Preprints, *12th Conf. on Severe Local Storms,* San Antonio, TX, Amer. Meteor. Soc., 422–424.

——, R. J. Donaldson Jr., and P. R. Desrochers, 1993: Tornado detection and warning by radar. *The Tornado: Its Structure, Dynamics, Prediction, and Hazards, Geophys. Monogr.,* No. 79, Amer. Geophys. Union, 203–221.

COMET, cited 1997: Mesoscale convective systems: Squall lines and bow echoes. Cooperative Program for Operational Meteorology Education and Training. [Available online at http://meted.ucar.edu/convection/mcs/mcsweb; CD-ROM version also available from UCAR/COMET, P.O. Box 3000, Boulder, CO 80307-3000.]

Davies-Jones, R. P., D. Burgess, and M. Foster, 1990: Test of helicity as a tornado forecast parameter. Preprints, *16th Conf. on Severe Local Storms,* Kananaskis Park, AB, Canada, Amer. Meteor. Soc., 588–592.

DeWald, V. L., T. W. Funk, J. D. Kirkpatrick, and Y.-J. Lin, 1998: The 18 May 1995 squall line over south-central Kentucky: An examination of complex storm reflectivity trends and multiple mesocyclone development. Preprints, *16th Conf. on Weather Analysis and Forecasting,* Phoenix, AZ, Amer. Meteor. Soc., 148–151.

Doswell, C. A., III, and D. W. Burgess, 1993: Tornadoes and tornadic storms: A review of conceptual models. *The Tornado: Its Structure, Dynamics, Prediction, and Hazards, Geophys. Monogr.,* No. 79, Amer. Geophys. Union, 161–172.

——, A. R. Moller, and R. Przybylinski, 1990: A unified set of conceptual models for variations on the supercell theme. Preprints, *16th Conf. on Severe Local Storms,* Kananaskis Park, AB, Canada, Amer. Meteor. Soc., 40–45.

Eilts, M. D., J. T. Johnson, E. D. Mitchell, R. J. Lynn, P. Spencer, S. Cobb, and T. M. Smith, 1996: Damaging downburst prediction and detection algorithm for the WSR-88D. Preprints, *18th Conf. on Severe Local Storms,* San Francisco, CA, Amer. Meteor. Soc., 541–545.

Forbes, G. S., and R. M. Wakimoto, 1983: A concentrated outbreak of tornadoes, downbursts and microbursts, and implications regarding vortex classification. *Mon. Wea. Rev.,* **111,** 220–235.

Fovell, R. G., and Y. Ogura, 1988: Numerical simulation of a midlatitude squall line in two dimensions. *J. Atmos. Sci.,* **45,** 3846–3879.

Fujita, T. T., 1978: Manual of downburst identification for Project NIMROD. SMRP No. 156, University of Chicago, 104 pp. [Available from Dept. of Geophysical Sciences, University of Chicago, Chicago, IL 60637.]

Funk, T. W., K. E. Darmofal, J. D. Kirkpatrick, M. T. Shields, R. W. Przybylinski, Y.-J. Lin, G. K. Schmocker, and T. J. Shea, 1996a: Storm reflectivity and mesocyclone evolution associated with the 15 April 1994 derecho, Part II: Storm structure and evolution over Kentucky and southern Indiana. Preprints, *18th Conf. on Severe Local Storms,* San Francisco, CA, Amer. Meteor. Soc., 516–520.

——, B. P. Smull, and J. D. Ammerman, 1996b: Structure and evolution of an intense bow echo embedded within a heavy rain producing MCS over Missouri. Preprints, *18th Conf. on Severe Local Storms,* San Francisco, CA, Amer. Meteor. Soc., 521–526.

——, V. L. DeWald, and Y.-J. Lin, 1998: A detailed WSR-88D Doppler radar evaluation of a damaging bow echo event on 14 May 1995 over north-central Kentucky. Preprints, *19th Conf. on Severe Local Storms,* Minneapolis, MN, Amer. Meteor. Soc., 436–439.

Hamilton, R. E., 1970: A review of the use of radar in detection of tornadoes and hail. ESSA Tech. Memo. WBTM-ER-34, 64 pp. [Available from NWS Eastern Region, Scientific Services Division, Bohemia, NY 11716.]

Heinlein, M. F., Jr., R. W. Przybylinski, and Y.-J. Lin, 1998: A WSR-88D Doppler radar study of an embedded bow echo event on 22 September 1993 over east-central Missouri. Preprints, *19th Conf. on Severe Local Storms,* Minneapolis, MN, Amer. Meteor. Soc., 522–525.

Houze, R. A., Jr., S. A. Rutledge, M. I. Biggerstaff, and B. F. Smull, 1989: Interpretation of Doppler weather radar displays of midlatitude mesoscale convective systems. *Bull. Amer. Meteor. Soc.,* **70,** 608–619.

Johns, R. H., 1993: Meteorological conditions associated with bow echo development in convective storms. *Wea. Forecasting,* **8,** 294–299.

——, and W. D. Hirt, 1987: Derechos: Widespread convectively induced windstorms. *Wea. Forecasting,* **2,** 32–49.

Lafore, J., and M. W. Moncrieff, 1989: A numerical investigation of the organization and interaction of the convective and stratiform regions of tropical squall lines. *J. Atmos. Sci.,* **46**, 521–544.

Lemon, L. R., and D. W. Burgess, 1992: Supercell associated deep convergence zone revealed by a WSR-88D. Preprints, *26th Conf. on Radar Meteorology,* Norman, OK, Amer. Meteor. Soc., 206–208.

——, and S. Parker, 1996: The Lahoma storm deep convergence zone: Its characteristics and role in storm dynamics and severity. Preprints, *18th Conf. on Severe Local Storms,* San Francisco, CA, Amer. Meteor. Soc., 70–75.

Moeller, A. R., C. A. Doswell III, M. P. Foster, and G. R. Woodall, 1994: The operational recognition of supercell thunderstorm environments and storm structures. *Wea. Forecasting,* **9,** 327–347.

Nelson, S. P., 1987: The hybrid multicellular–supercellular storm—An efficient hail producer. Part II: General characteristics and implications for hail growth. *J. Atmos. Sci.,* **44,** 2060–2073.

Nolen, R. H., 1959: A radar pattern associated with tornadoes. *Bull. Amer. Meteor. Soc.,* **40,** 277–279.

Przybylinski, R. W., 1995: The bow echo: Observations, numerical simulations, and severe weather detection methods. *Wea. Forecasting,* **10,** 203–218.

——, and G. K. Schmocker, 1993: The evolution of a widespread convective windstorm event over central and eastern Missouri. Preprints, *13th Conf. on Weather Analysis and Forecasting,* Vienna, VA, Amer. Meteor. Soc., 461–465.

——, Y.-J. Lin, G. K. Schmocker, and T. J. Shea, 1995: The use of realtime WSR-88D, profiler, and conventional data sets in forecasting a northeastward moving derecho over eastern Missouri and central Illinois. Preprints, *14th Conf. on Weather Analysis and Forecasting,* Dallas, TX, Amer. Meteor. Soc., 335–342.

——, Y.-J. Lin, C. A. Doswell III, G. K. Schmocker, T. J. Shea, T. W. Funk, K. E. Darmofal, J. D. Kirkpatrick, and M. T. Shields, 1996: Storm reflectivity and mesocyclone evolution associated with the 15 April 1994 derecho, Part I: Storm structure and evolution over Missouri and Illinois. Preprints, *18th Conf. on*

Severe Local Storms, San Francisco, CA, Amer. Meteor. Soc., 509–515.

Rotunno, R., J. B. Klemp, and M. L. Weisman, 1988: A theory for strong, long-lived squall lines. *J. Atmos. Sci.*, **45,** 463–485.

Rutledge, S. A., R. A. Houze, M. I. Biggerstaff, and T. Matejka, 1988: The Oklahoma–Kansas mesoscale convective system of 10–11 June 1985: Precipitation structure and single-Doppler radar analysis. *Mon. Wea. Rev.*, **116,** 1409–1430.

Schmocker, G. K., R. W. Przybylinski, and Y.-J. Lin, 1996: Forecasting the initial onset of damaging downburst winds associated with a mesoscale convective system (MCS) using the mid-altitude radial convergence (MARC) signature. Preprints, *15th Conf. on Weather Analysis and Forecasting,* Norfolk, VA, Amer. Meteor. Soc., 306–311.

Sohl, C. J., E. M. Quetone, and L. R. Lemon, 1996: Severe storm warning decisions: Operational impact of multiple radars. Preprints, *18th Conf. on Severe Local Storms*, San Francisco, CA, Amer. Meteor. Soc., 560–564.

Smull, B. F., and R. A. Houze Jr., 1987: Rear inflow in squall lines with trailing stratiform precipitation. *Mon. Wea. Rev.,* **115,** 2869–2889.

Wakimoto, R. M., and J. W. Wilson, 1989: Non-supercell tornadoes. *Mon. Wea. Rev.*, **117,** 1113–1140.

Weismann, M. L., 1992: The role of convectively generated rear-inflow jets in the evolution of long-lived mesoconvective systems. *J. Atmos. Sci.,* **49,** 1826–1847.

——, 1993: The genesis of severe, long-lived bow echoes. *J. Atmos. Sci.,* **50,** 645–670.

——, and J. B. Klemp, 1982: The dependence of numerically simulated convective storms on vertical wind shear and buoyancy. *Mon. Wea. Rev.*, **110,** 504–520.

——, and ——, 1984: The structure and classification of numerically simulated convective storms in directionally varying wind shears. *Mon. Wea. Rev.,* **112,** 2479–2498.

Wood, V. T., 1996: Effects of radar sampling on Doppler velocity tornadic vortex signatures. Preprints, *18th Conf. on Severe Local Storms,* San Francisco, CA, Amer. Meteor. Soc., 577–580.